Research Article | Vol. 8, No. 8 | 1 Aug 2017 | BIOMEDICAL OPTICS EXPRESS 3807

Biomedical Optics EXPRESS

Line scanning, stage scanning confocal microscope (LSSSCM)

DANIEL S. GAREAU,[1,*] JAMES G. KRUEGER,[1] JASON E. HAWKES,[1] SAMANTHA R. LISH,[1] MICHAEL P. DIETZ,[1] ALBA GUEMBE MÜLBERGER,[1] EUPHEMIA W. MU,[2] MARY L. STEVENSON,[2] JESSE M. LEWIN,[3] SHANE A. MEEHAN,[2] AND JOHN A. CARUCCI[2]

[1] *Investigative Dermatology, The Rockefeller University, 1230 York Ave., New York, NY 10065, USA*
[2] *Ronald O. Pearleman Department of Dermatology, New York University, 240 E. 38th St., New York, NY 10016, USA*
[3] *Department of Dermatology, Columbia University Medical Center, 161 Fort Washington Avenue, 12th Floor, New York, NY 10032, USA*
[*] *dgareau@rockefeller.edu*
http://dangareau.net

Abstract: For rapid pathological assessment of large surgical tissue excisions with cellular resolution, we present a line scanning, stage scanning confocal microscope (LSSSCM). LSSSCM uses no scanning mirrors. Laser light is focused with a single cylindrical lens to a line of diffraction-limited width directly into the (Z) sample focal plane, which is parallel to and near the flattened specimen surface. Semi-confocal optical sections are derived from the linear array distribution (Y) and a single mechanical drive that moves the sample parallel to the focal plane and perpendicular to the focused line (X). LSSSCM demonstrates cellular resolution in the conditions of high nuclear density within micronodular basal cell carcinoma.

© 2017 Optical Society of America

OCIS codes: (110.0180) Microscopy; (170.1790) Confocal microscopy; (170.1870) Dermatology; (170.5810) Scanning microscopy; (170.7050) Turbid media.

References and links

1. M. Rajadhyaksha, R. R. Anderson, and R. H. Webb, "Video-rate confocal scanning laser microscope for imaging human tissues in vivo," Appl. Opt. **38**, 2105–2115 (1999).
2. H. W. Rogers, M. A. Weinstock, S. R. Feldman, and B. M. Coldiron, "Incidence Estimate of Non-melanoma Skin Cancer (Keratinocyte Carcinomas) in the US Population, 2012," JAMA Dermatol. **151**, 1081–1086 (2015).
3. S. M. Connolly, D. R. Baker, B. M. Coldiron, M. J. Fazio, P. A. Storrs, A. T. Vidimos, M. J. Zalla, J. D. Brewer, W. Smith Begolka, P. Ratings, T. G. Berger, M. Bigby, J. L. Bolognia, D. G. Brodland, S. Collins, T. A. Cronin, Jr., M. V. Dahl, J. M. Grant-Kels, C. W. Hanke, G. J. Hruza, W. D. James, C. W. Lober, E. I. McBurney, S. A. Norton, R. K. Roenigk, R. G. Wheeland, and O. J. Wisco, "AAD/ACMS/ASDSA/ASMS 2012 appropriate use criteria for Mohs micrographic surgery: a report of the American Academy of Dermatology, American College of Mohs Surgery, American Society for Dermatologic Surgery Association, and the American Society for Mohs Surgery," J. Am. Acad. Dermatol. **67**, 531–550 (2012).
4. A. K. El Tal, A. E. Abrou, M. A. Stiff, D. A. Mehregan, "Immunostaining in Mohs micrographic surgery: a review," Dermatolgic Surgery **36**(3), 275–90 (2010).
5. M. Titford. "The long history of hematoxylin," Biotech. Histochem. **80**(2), 73–78 (2005).
6. M. S. Shareef and W. Hussain, "The Mohs histotechnician: a review of training and practice within 29 centres in the UK," Clinical and Experimental Dermatology **38**, 589–593 (2013).
7. R. S. Stern, "Cost effectiveness of Mohs micrographic surgery," J. Investigative Dermatology **133**, 1129–1131 (2013).
8. J. K. Karen, D. S. Gareau, S. W. Dusza, M. Tudisco, M. Rajadhyaksha, and K. S. Nehal, "Detection of basal cell carcinomas in Mohs excisions with fluorescence confocal mosaicing microscopy," Br. J. Dermatol. **160**, 1242–1250 (2009).
9. D. Gareau, A. Bar, N. Snaveley, K. Lee, N. Chen, N. Swanson, E. Simpson, and S. Jacques, "Tri-modal confocal mosaics detect residual invasive squamous cell carcinoma in Mohs surgical excisions," J. Biomed. Opt. **17**, 066018 (2012).
10. A. Bennassar, A. Vilata , S. Puig , and J. Malvehy, "Ex vivo fluorescence confocal microscopy for fast evaluation of tumour margins during Mohs surgery," Br. J. Dermatol. **170**(2), 360–365 (2014).
11. R. M. Campbell, C. S. Perlis, M. K. Malik, and R. G. Dufresne, Jr., "Characteristics of Mohs practices in the United States: a recall survey of ACMS surgeons," Dermatologic Surgery **33**, 1413–1418 (2007).

#295944 https://doi.org/10.1364/BOE.8.003807
Journal © 2017 Received 18 May 2017; revised 7 Jul 2017; accepted 8 Jul 2017; published 24 Jul 2017

Biomedical Optics EXPRESS

12. D. S. Gareau, Y. Li, B. Huang, Z. Eastman, K. S. Nehal, and M. Rajadhyaksha, "Confocal mosaicing microscopy in Mohs skin excisions: feasibility of rapid surgical pathology," J. Biomed. Opt. **13**, 054001 (2008).
13. D. S. Gareau, "Feasibility of digitally stained multimodal confocal mosaics to simulate histopathology," J. Biomed. Opt. **14**, 034050 (2009).
14. D. S. Gareau, J. K. Karen, S. W. Dusza, M. Tudisco, K. S. Nehal, and M. Rajadhyaksha, "Sensitivity and specificity for detecting basal cell carcinomas in Mohs excisions with confocal fluorescence mosaicing microscopy," J. Biomed. Opt. **14**, 034012 (2009).
15. E. W. Mu, J. M. Lewin, M. L. Stevenson, S. A. Meehan, J. A. Carucci, and D. S. Gareau, "Use of Digitally Stained Multimodal Confocal Mosaic Images to Screen for Nonmelanoma Skin Cancer," JAMA Dermatol. **152**, 1335–1341 (2016).
16. D. S. Gareau, H. Jeon, K. S. Nehal, and M. Rajadhyaksha, "Rapid screening of cancer margins in tissue with multimodal confocal microscopy," J. Surg. Res. **178**, 533–538 (2012).
17. M. Rajadhyaksha, M. Grossman, D. Esterowitz, R. H. Webb, and R. R. Anderson, "In vivo confocal scanning laser microscopy of human skin: melanin provides strong contrast," The Journal of investigative dermatology **104**, 946–952 (1995).
18. K. B. Im, S. Han, H. Park, D. Kim, and B. M. Kim, "Simple high-speed confocal line-scanning microscope," Opt. Express **13**, 5151–5156 (2005).
19. R. Wolleschensky, B. Zimmermann, and M. Kempe, "High-speed confocal fluorescence imaging with a novel line scanning microscope," J. Biomed. Opt. **11**, 064011 (2006).
20. T. Yang, T. Zheng, Z. Shang, X. Wang, X. Lv, J. Yuan, and S. Zeng, "Rapid imaging of large tissues using high-resolution stage-scanning microscopy," Biomed. Opt. Express **6**, 1867–1875 (2015).
21. K. V. Vienola, M. Damodaran, B. Braaf, K. A. Vermeer, and J. F. de Boer, "Parallel line scanning ophthalmoscope for retinal imaging," Opt. Lett. **40**, 5335–5338 (2015).
22. D. S. Gareau, S. Abeytunge, and M. Rajadhyaksha, "Line-scanning reflectance confocal microscopy of human skin: comparison of full-pupil and divided-pupil configurations," Opt. Lett. **34**, 3235–3237 (2009).
23. Y. G. Patel, K. S. Nehal, I. Aranda, Y. Li, A. C. Halpern, and M. Rajadhyaksha, "Confocal reflectance mosaicing of basal cell carcinomas in Mohs surgical skin excisions," J. Biomed. Opt. **12**, 034027 (2007).
24. S. Abeytunge, Y. Li, B. Larson, G. Peterson, E. Seltzer, R. Toledo-Crow, and M. Rajadhyaksha, "Confocal microscopy with strip mosaicing for rapid imaging over large areas of excised tissue," J. Biomed. Opt. **18**, 61227 (2013).
25. *Reflectance Confocal Microscopy for Skin Diseases* R. Hofmann-Wellenhof, G. Pellacani, J. Malvehy, H. P. Soyer, eds. (Springer, 2012).
26. Caliber ID Inc. Technical Note on RS-G4 imager 2017 [cited 2017 07-04-2017]. Available from: http://www.caliberid.com/RS-G4-Technote0217.pdf
27. R. M. Levenson and F. Fereidouni, "MUSE: A New, Fast, Simple Microscopy Method for Slide-Free Histology and Surface Topography," The FASEB Journal **30**(51.53) (2016).

1. Introduction

1.1. Historical context

Video-rate microscopy introduced the potential for confocal point-scanning, rapid bedside pathology in 1999 [1]. Expedited pathology by confocal imaging may aid a wide range of specialty practices where the goal is complete tumor resection verified by negative margins. Figure 1 shows that the majority of the 6 million new cancer cases per year in the US are non-melanoma skin cancers (e.g. basal cell carcinoma, BCC or squamous cell carcinoma, SCC). [2] 25% of non-melanoma skin cancers are treated with Mohs micrographic surgery [3] because they possess a high risk of recurrence or occur on functionally sensitive areas such as the face. Mohs surgery is a tissue-sparing procedure indicated for the treatment of non-melanoma skin cancers. Mohs micrographic surgery achieves the highest cure rate for non-melanoma skin cancers because it allows for complete margin analysis at the time of surgery. The limiting factor for Mohs surgery is frozen section pathology [4], which is hundreds of years old [5] and requires extensive processing of the tissue specimen. [6] [7]

1.2. Unmet clinical need

Rapid confocal pathology may provide: 1) more efficient patient care, 2) facilitated margin control by simplified specimen orientation maintenance, 3) improved functional outcome due to enhanced micrographic precision, and 4) enhanced patient experience with reduced anxiety. The Mohs procedural time would be reduced by almost two thirds if standard histopathology

Biomedical Optics EXPRESS

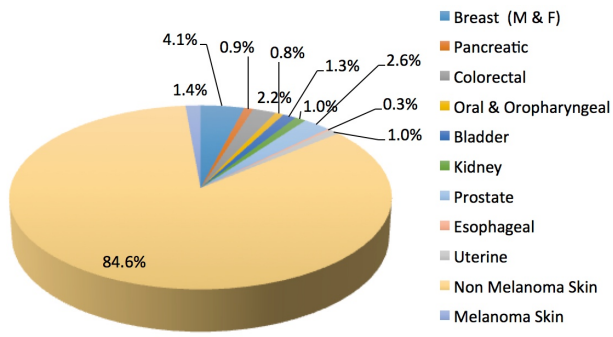

Fig. 1. Cancer incidence rates in the United States. 5.4 million [3] of the 6 million new cancer cases in the US are the non-melanoma skin cancers that confocal point scanning systems have proven effective in detecting: Basal Cell Carcinoma (BCC) [8] and Squamous Cell Carcinoma (SCC). [9]

could be replaced with rapid confocal pathology. [10] Considerable interdisciplinary research has been performed between engineers adapting the point-scanning confocal imager [1] and members of the key potential early-adopter community, which includes dermatologists and Mohs surgeons. [11] Confocal microscopy can be used as a dermatopathology tool on whole, freshly-excised tissue specimens. Multimodal imaging technology has been developed [12] [13] and has demonstrated sensitive and specific margin screening. [8] [9] [10] [14] [15] [16]

Towards a less complicated, less expensive, and less delicate device, line scanning confocal microscopy modifies the point scanning design [17] by replacing point illumination and point detection with line illumination and line detection, respectively. [18] [19] [20] In contrast to the point scanning system [1] [12] and other commercial line scanners [21], we present a line scanner that uses no moving optics or coupling media, which may help optimize manufacture. In this paper, we demonstrate cellular resolution for the LSSSCM as a first step towards a study of the sensitivity and specificity of margin screening using this device.

1.3. Geometric optics, cellular resolution

In point-scanning, the point must be scanned in both directions, typically with a pair of mirrors: a galvanometric mirror for the slow axis and a polygon mirror for the fast axis. In the LSSSCM, lines are recorded simultaneously on an array detector, which eliminates the need to optically scan the beam in the non-confocal Y-direction at the cost of reducing the resolution (ΔY, Eq. (2)). The field of view in the direction of the focused line can be as long as the line itself (6mm in our system) and can be very long in the direction of the physical scanning of the stage (3cm in our system). In our design (Fig. 2) the line illumination is achieved with a single cylindrical lens. Line detection is achieved with a confocal linear array detector.

The diffraction-limited line-width of 488nm illumination in the sample focal plane is 6μm, where the detector elements sample 1 square μm. The predicted diffraction-limited lateral resolution element in the imaging light path. This is 1/2 the size of the Airy Unit = 1.22λ/NA for Niquist sampling where NA is the objective lens numerical aperture, and for our system is given [22] by Eqs. (1) and (2).

$$\Delta Y = \frac{0.79\lambda}{NA} = \frac{0.79 \times 488nm}{0.28} = 1.37\mu m \tag{1}$$

$$\Delta X = \frac{0.61\lambda}{NA} = \frac{0.61 \times 488nm}{0.28} = 1.06\mu m \tag{2}$$

Biomedical Optics EXPRESS

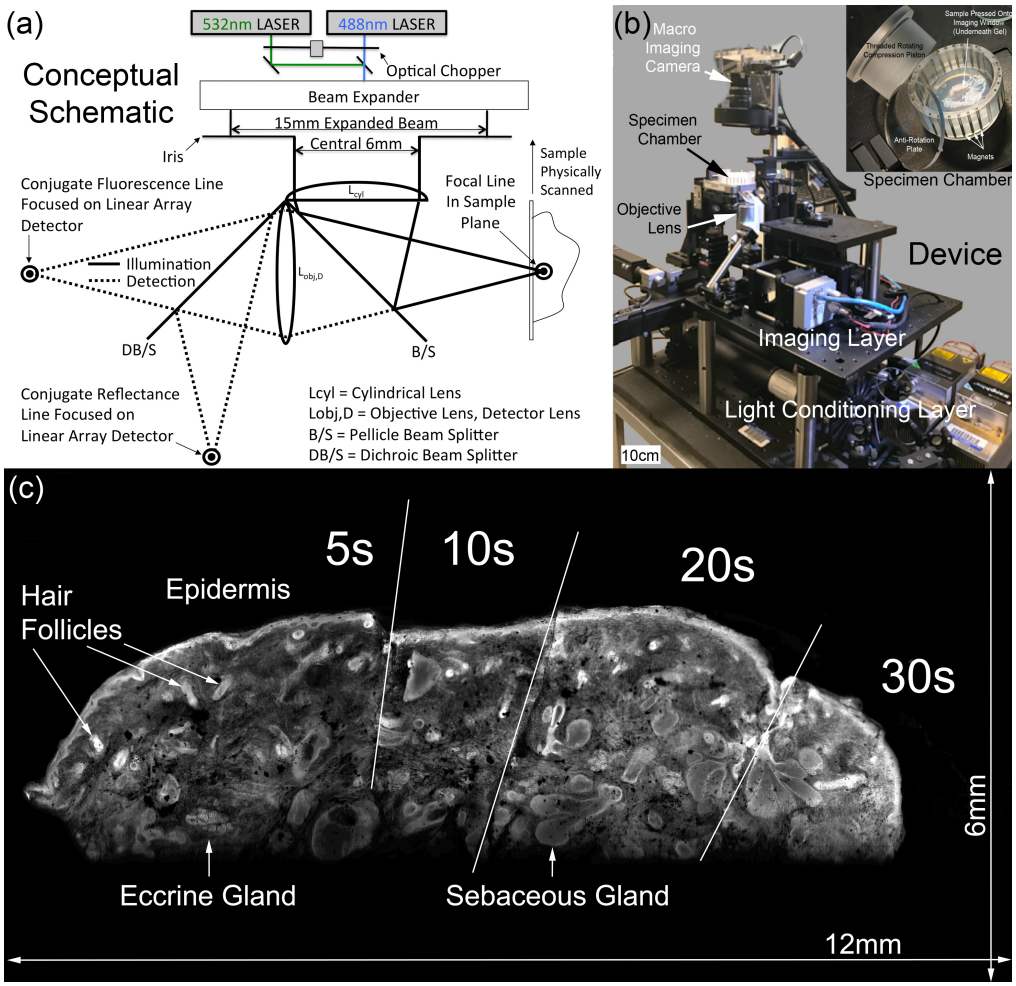

Fig. 2. Stage-Scanning, Line Scanning Confocal Microscope in concept (a) and physical embodiment (b). The experimental result sample image (c) shows a 12-mm horizontal field of view scanned in 2 minutes without mosaicking. The sample has been cut into 4 pieces, stained (with various immersion times of 5, 10, 20 and 30 seconds) in 1mM acridine orange solution (pH=6.0), and re-assembled for imaging.

2. Methods

2.1. Instrumentation

Illumination consists of 300mW, 488nm and 532nm Coherent Sapphire LASERs (Coherent Inc., Santa Clara, CA). The LASER beams are expanded to a diameter of 15mm such that only the central, relatively flat portion of the Gaussian radial light distribution profile becomes the 6mm-long focused, illumination line. The 488nm and 532nm illumination LASER light is processed by an optical chopper (MC2000B, Thorlabs, Newtown NJ) to allow one beam or the other to transmit toward the beam expander in alternating periods of equal duration. Upon exiting the beam expander, the expanded, time-modulated illumination beam is focused to a line directly onto the sample focal plane using a cylindrical lens (ACY254-050-A, focal length (F_c)=50mm Thorlabs, Newtown NJ). The theoretically predicted full width at half maximum ($FWHM$) of the focused line in the sample focal plane resulting from the diameter (D)=6mm beam focused

Biomedical Optics EXPRESS

through the cylindrical lens is given by:

$$FWHM = \frac{1.22\lambda \frac{F_c}{D}}{0.849} = 5.84\mu m \tag{3}$$

The illumination path includes no spherical optics, so field curvature is limited to that of the objective lens in the detection path. The 6mm-long line in the sample focal plane is optically conjugated onto a linear array detector by an objective lens and a detector lens with infinity space between the two lenses. Stage translation steps of 1μm are timed with sequential line captures to build up an image of the tissue block face. Figure 2(a) shows a conceptual diagram of the LSSSCM system. The simplified diagram is physically accurate with the following three refinements: (1) the objective and detector lenses are shown as one design element when they are physically separate components, (2) the dichroic beam splitter (which separates the reflectance and fluorescence detection paths) is in the infinity space between the objective lens and the detector lens, not in the focusing light path to the detector as drawn in the figure, and (3) there is a barrier filter (FF01-515/588/700-50, Semrock, Inc. Rochester, NY), that blocks excess reflectance light from the fluorescence detector, which is also located in the infinity space (not shown in the figure) between the objective and detector lenses.

2.2. Illumination & detection

Both the objective and cylindrical lenses focus in the sample focal plane. The (focusing) illumination and (diverging) detection beam paths are combined by the pellicle beam splitter (National Photocolor, Mamaroneck, NY) in the space between the pellicle beam splitter and the sample. Detected light is transmitted back through the pellicle beam splitter such that the objective lens (20X G Plan Apo T=3.5mm, EFL=10.0mm, Mitutoyo, Aurora, IL) can be positioned out of the illumination path. Upon exiting the back aperture of the objective lens, fluorescent and reflected light are separated using a dichroic mirror (Di01-R405/488/532/635-25x36, Semrock Inc., Rochester, NY). The dichroic beam-splitter, which is thick (1.5mm) relative to the pellicle beam splitter (3μm), is located in the infinity space between the infinity-corrected objective and detector lenses to avoid aberrations, whereas the pellicle was chosen for its thin (non-abberating) property in the focal path of the objective lens. In each detection path (reflectance and fluorescence), the same lens/detector pair measures the relevant signal. The detector lens (49-292-INK, Edmund Optics, EFL=75.0mm Barrington, NJ) and line detector (105995, Basler Inc., Exton, PA) are identical for the fluorescence and reflection channels.

2.3. Scanning

The LSSSCM design differs from the previously tested point-scanning system in that it is low-NA imaging without immersion media, it is non-confocal in the direction of the line, and it completely lacks scanning mirrors. We believe these differences, if proven to enable cellular pathological analysis, will lead to a better technology for rapid margin screening in staged cancer excisions.

A 3D translation stage (LNR50S for X and Y, DRV001 for Z, Thorlabs, Newtown NJ) magnetically couples to a custom tissue compression chamber. The tissue compression chamber (Fig. 2b), which is based on a previous design [23], features a 3mm-thick, 3cm-diameter circular imaging window, the surgical specimen, an agarose gel disc, a polycarbonate window with protruding tabs that mate with notches in the chamber to prevent torsion, a threaded piston for rotational compression and 24 cylindrical neodymium magnets (D16, K&J Magnetics, Pipersville, PA) that mechanically fix the chamber to the magnetic kinematic mount (Custom KS2D machined from stainless steel to be magnetic, Thorlabs, Newtown NJ). The magnets embedded in the tissue compression chamber enable the mounted specimen to be easily placed

Biomedical Optics EXPRESS

and magnetically locked into the microscope. The stage is controlled through a 3-axis control system (BSC203, Thorlabs, Newtown NJ).

All confocal illumination and detection is achieved in the inverted, epi-fluorescent configuration while on the other side of the sample, a standard camera system (SMN-B050-U B/W camera, Mightex Inc., Toronto ON, CA, coupled with 56-787 lens, Edmund Optics, Barrington, NJ) images the entire tissue compression under LED illumination in an upright configuration. A graphic user interface (GUI) written in Matlab (Mathworks, Natick MA) enables targeting of the region of interest by the standard camera so that the line can be directed to scan only the targeted area in confocal modes. Matlab communication with the cameras as Video Objects was developed in collaboration with Mathworks, available in the 2016b Matlab release. The multifunctional graphic user interface enables functions such as live line readouts at ~1KHz for alignment. The interface features macroscopic image acquisition from above the sample such that coordinates can be entered via mouse clicks or touch screen that restrict the scan range to the spatial extent of the sample. The digital "frame grabber," implemented in Matlab, clocks the optical chopper and separates sequentially acquired lines into four separate image frames at each stage movement position: fluorescence and reflectance at the 488nm and 532nm illumination wavelengths. The dual wavelength design is chosen to support differential nuclear/cytoplasmic (acridine orange/eosin) fluorescence labeling. [9] This report, mirroring the original point scanning BCC study [12], demonstrates easily recognizable pathologic cellular morphology of BCC specimens, e.g. Fig. 4(a), imaged in fluorescence mode with 488nm-excited nuclear labeling.

3. Results

3.1. System characterization

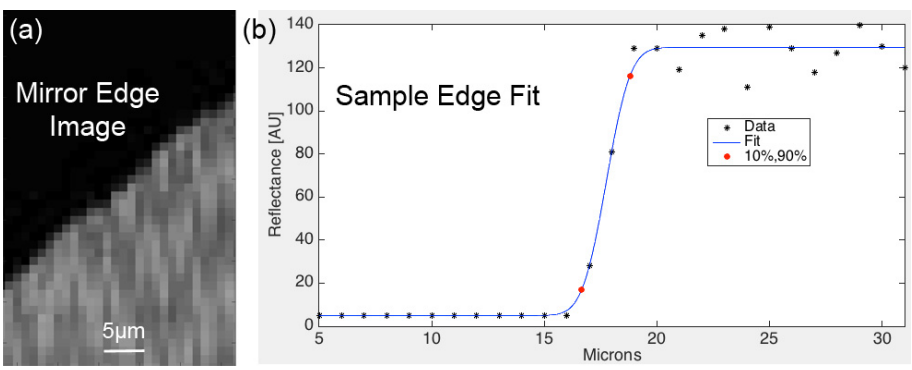

Fig. 3. Image analysis of mirrored grating target. The image (a) is sampled along a single X or Y position to extract pixel values (b, black *) that comprise an edge trace which is fit using a sigmoidal function (b, blue line) that specifies the 10% and 90% brightness coordinates (b, red *).

The magnification of the system is 75mm/10mm, so the 7μm square pixels of the line camera each conjugate to approximately a 1μm spot in the sample focal plane. This configuration slightly under-samples the detection path lateral resolution elements (Eqs. (1) and (2)) according to Niquist criteria. X and Y-lateral resolution was measured with a reflective Ronchi Ruling grating target in the sample focal plane, sampling image pixels across reflective edges in the respective directions. Pixel samples in columns and rows were fit with a sigmoidal function that traced across the reflective edge. The fitting results, e.g. Fig. 3, yielded the lateral distance between the 10% and 90% reflectance levels of reflectance of $W_{x10:90} = 1.3 \pm 0.6\mu m$ and $W_{y10:90} = 2.0 \pm 0.8\mu m$ (n=15) with variance due to mirror reflection interference. The axial

line-spread function was also measured to be 13.4 ± 0.8μm (n=15).

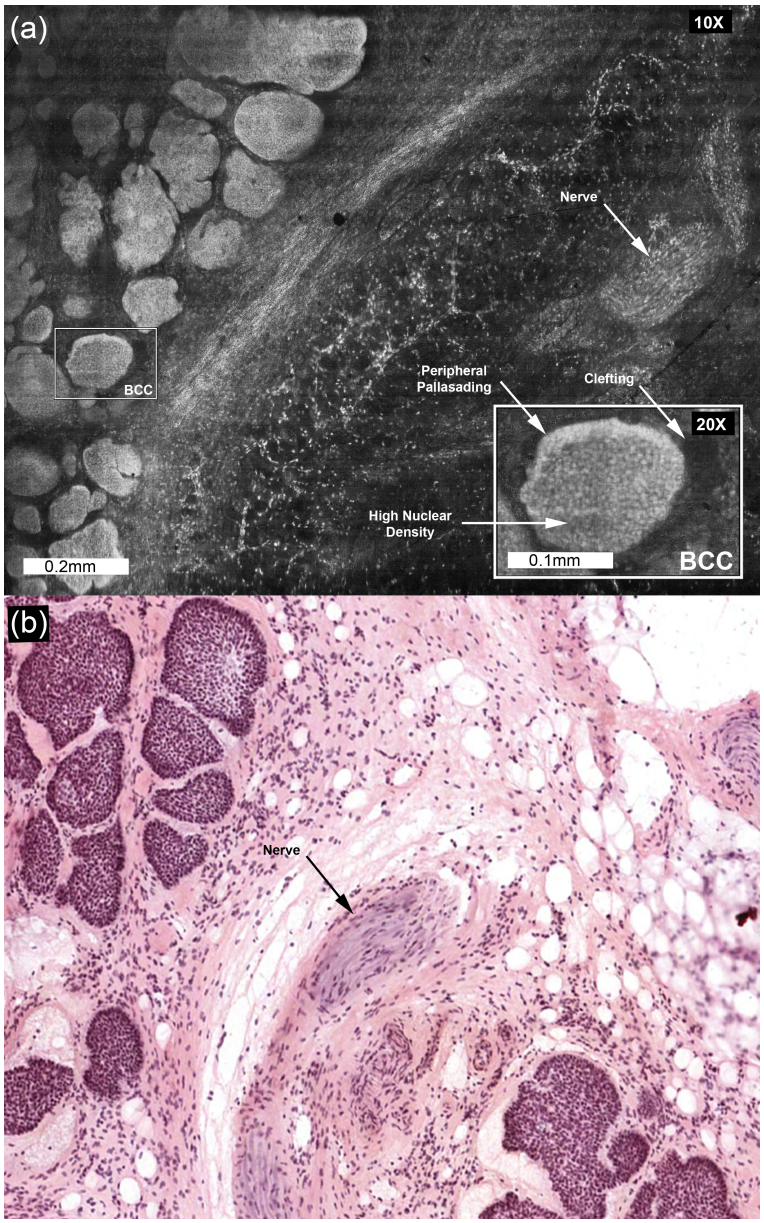

Fig. 4. Confocal image of basal cell carcinoma (BCC), acquired 10μm beneath the surface of a 4mm-thick tissue specimen with correlating histology. The inset shows a magnified view of a single tumor with characteristic pathologic features identified.

3.2. Tissue imaging

Surgically excised and discarded specimens of BCC were obtained under the written, informed consent of 22 patients under Institutional Review Board-approved protocols at The Rockefeller University and New York University. Specimens were stained with acridine orange 1mM in phosphate buffered saline at pH 6.0 for 30 seconds prior to imaging. Experimental images were

Biomedical Optics EXPRESS

acquired at a stage translation speed of 1mm per 10 seconds, so a scan such as in Fig. 2(c) was achieved in 2 minutes. Fluorescence mode images under 488nm illumination show cellular resolution and contrast comparable to the previous point scanning instrumentation. [12]

Figure 4 shows a sample image of a BCC specimen. The full 6mm-square field of view is cropped such that the vertical dimension shown is the central 2mm of the 6mm field of view. Images from the first 10 specimens were acquired while the microscope was still being engineered, and the resolution was insufficient for analysis of cellular detail. 10 of the 12 images acquired after the LSSSCM design was frozen for optimal alignment and resolution showed good or excellent resolution and contrast. In the two images that were of poor quality, misalignments caused insufficient resolution of individual cells such that greater structures (tumor nodules, sebaceous glands, etc.) were recognizable, but the cells therein were un-resolvable.

4. Discussion

4.1. Translational context

The early and accurate diagnosis of skin cancer represents a significant, on-going challenge for clinicians. A tremendous diagnostic gap exists between traditional non-destructive screening techniques for skin lesions (e.g. full-body skin photography or dermoscopy) and histopathologic examination. This gap is due to a variety of factors including the experience of the examiner, the evaluation of lesions that lack disease-specific clinical features, and the inability to detect skin features at the cellular level. The introduction of reflectance confocal microscopy (RCM) technology [25] helped close this diagnostic gap by allowing clinicians to visualize the skin at the cellular level *in vivo* without the need for biopsy or excision. However, a major limitation of RCM is nonspecific reflectance contrast. LSSSCM overcomes this limitation by imaging on freshly excised specimens and, therefore, can potentially bridge the gap between clinical screening and histopathologic analysis.

4.2. Summary of this research

LSSSCM, an application-specific confocal embodiment, minimizes electro-optical complexity, maximizes scan speed, and minimizes the need for mosaicking during potential diagnostic evaluation of tissue specimens. LSSSCM is a promising candidate for clinical translation of rapid pathology and surgical guidance given the clinical demand (Fig. 1), the elegant, portable design (Fig. 2), the potential multimodality, supporting hematoxalyn and eosin-like colorization [13], and the increasing scan speeds (**Table 1**) of confocal microscopy. Notable design elements include the separate illumination and detection paths, the low NA, air-coupled objective lens and the custom tissue compression chamber for mounting specimens. LSSSCM achieves cellular resolution and shows cellular morphology (Fig. 4) with nuclear contrast and, therefore, has the potential to support sensitive and specific, high-throughput pathologic screening of residual cancer in tissue specimens. Ongoing studies aim to evaluate the diagnostic accuracy of LSSSCM in terms of its sensitivity and specificity. Additional efforts include speed optimization to enable faster image acquisition, re-engineering the physical device to achieve a more compact format, and real-time amalgamation of all four imaging modes which will enable colorized multimodal images that approximate the appearance of standard H&E histology. [9]

4.3. Technologies competing for speed

LSSSCM currently images at a 100Hz line acquisition rate. Since the maximum line acquisition rate for the LSSSCM cameras is 170 times faster, system optimization for high-throughput imaging is a goal of future work. The scanned area in Fig. 2(c) of 12mm $\times$ 6mm = 72mm^2 scanned in 2 minutes demonstrates a surface area scan rate of 0.60mm^2 per second. This rate is faster than the specified scan rate (0.30mm^2 per second: 5mm $\times$ 5mm in 84 seconds) [26] for a

Biomedical Optics EXPRESS

commercially available point-scanning confocal microscope (RS-G4, Caliber ID, Rochester, NY). Point scanning technology is able to scan faster (0.56mm^2 per second: 10mm × 10mm in 180 seconds) in a research version of the device using point-scanning, strip mosaicking mode. [24] The fastest reported scan rate is from a similar rapid line-scanning system (0.88mm^2 per second: 10mm × 10mm in 88 seconds) [20] using a 40-times, water immersion, 0.8 NA objective lens and the same 488nm LASER wavelength. In their system, 1 Airy unit is 0.74 μm so the illumination point spread function (PSF) is superior to (Eq. (3)) the one in this work. The PSF full width at half maximum in the X and Y directions are 0.47 μm ± 0.02 μm and 0.56 μm ± 0.01 μm(n = 5) in their system, respectively. Table 1 summarizes the scan speeds of the various competing technologies.

Table 1. Scan Speed of Competing Technologies

Technology	Reference	Surface Area (time)	Area Scan Speed
Line Scanner	[20]	10mm×10mm (88s)	0.88mm^2 per second
LSSSCM	This Paper	12mm×6mm (120s)	0.60mm^2 per second
Point Scanner	[24]	10mm×10mm (180s)	0.56mm^2 per second
Point Scanner	[26]	5mm×5mm (84s)	0.30mm^2 per second

An additional factor impacting utility and overall procedure speed is an automated adjustment of sample tip and tilt. This must be done precisely (5μm tip/tilt tolerance over the lateral 3cm field of view) and currently requires 5 minutes using manual micrometer adjustment and feedback from live line readouts.

A non-confocal competing technology is block-face imaging by LED illumination fluorescence imaging microscopy. [27] Its surface sectioning derives from short wave ultra violet illumination. Its advantage is the speed derived from using the rectangular sensor array, versus our linear array here, and the need to physically translate the microscope stage. A potential disadvantage is that this device may fail to reject background scattered light for limited performance in highly scattering tissue like skin.

Funding

National Institutes of Health (R01CA193390, UL1TR001866, KL2TR001865); The Robertson Therapeutics Development Fund.

Acknowledgments

The content is solely the responsibility of the authors and does not necessarily represent the official views of the National Institutes of Health. The authors wish to thank Andrei Ursache and Ranjani Rajagopalan at Mathworks Inc. for developing Matlab upgrades to support the Basler cameras, Rio Butler for computer-automated design and mechanical engineering support, George Chen at Navitar (Special Optics) Inc. for providing standard geometric optics equations, and Vita Scaglione and Ron Nelson for help in constructing the pie chart in Fig. 1.

Disclosures

DSG: (P)